Published in final edited form as:
J Comp Neurol. 2013 April 15; 521(6): 1268–1288. doi:10.1002/cne.23226.

Genetic Labeling of Steroidogenic Factor-1 (SF-1) Neurons in Mice Reveals Ventromedial Nucleus of the Hypothalamus (VMH) Circuitry Beginning at Neurogenesis and Development of a Separate Non-SF-1 Neuronal Cluster in the Ventrolateral VMH

Clement C. Cheung[1,*], **Deborah M. Kurrasch**[2], **Jenna K. Liang**[1], and **Holly A. Ingraham**[3,*]

[1]Department of Pediatrics, University of California, San Francisco, California 94143

[2]Department of Medical Genetics, Faculty of Medicine, University of Calgary, Calgary, Alberta T2N 4N1, Canada

[3]Department of Cellular and Molecular Pharmacology, University of California, San Francisco, California 94143

Abstract

The ventromedial nucleus of the hypothalamus (VMH) influences a wide variety of physiological responses. Here, using two distinct but complementary genetic tracing approaches in mice, we describe the development of VMH efferent projections, as marked by steroidogenic factor-1 (SF-1; NR5A1). SF-1 neurons were visualized by Tau-green fluorescent protein (GFP) expressed from the endogenous *Sf-1* locus (*Sf-1*^{TauGFP}) or by crossing the transgenic *Sf1:Cre* driver to a GFP reporter strain (*Z/EG*$^{Sf1:Cre}$). Strikingly, VMH projections were visible early, at embryonic (E) 10.5, when few postmitotic SF1 neurons have been born, suggesting that formation of VMH circuitry begins at the onset of neurogenesis. At E14.5, comparison of these two reporter lines revealed that SF1-positive neurons in the ventrolateral VMH (VMH_{vl}) persist in *Z/EG*$^{Sf1:Cre}$ embryos but are virtually absent in *Sf-1*^{TauGFP}. Therefore, although the entire VMH including the VMH_{vl} shares a common lineage, the VMH_{vl} further differentiates into a neuronal cluster devoid of SF-1. At birth, extensive VMH projections to broad regions of the brain were observed in both mouse reporter lines, matching well with those previously discovered by injection of axonal anterograde tracers in adult rats. In summary, our genetic tracing studies show that VMH efferent projections are highly conserved in rodents and are established far earlier than previously appreciated. Moreover, our results imply that neurons in the VMH_{vl} adopt a distinct fate early in

*CORRESPONDENCE TO: Clement C. Cheung, Department of Pediatrics, University of California, San Francisco, CA 94143. ccheung@chla.usc.edu; or Holly A. Ingraham, Department of Cellular and Molecular Pharmacology, San Francisco, CA 94343. holly.ingraham@ucsf.edu.

AUTHOR CONTRIBUTIONS

All authors had full access to all the data in the study and take responsibility for the integrity of the data and the accuracy of data analysis. Study concept and design: CC, DK, and HI. Acquisition of data: CC, DK, and JL. Analysis and interpretation of data: CC, DK, and HI. Drafting of manuscript: CC and HI. Critical revision of the manuscript for important intellectual content: CC, DK, and HI.

CONFLICT OF INTEREST STATEMENT

The authors have no conflict of interest and nothing to disclose.

development, which might underlie the unique physiological functions associated with this VMH subregion.

INDEXING TERMS

VMH; SF-1; ventrolateral VMH; neurocircuitry; SF-1:Cre driver; GFP labeling; genetic tracing; ventral supraoptic commissure

The hypothalamus is the homeostatic center of the central nervous system and is composed of multiple nuclei. Among these, the ventromedial nucleus of the hypothalamus (VMH) is known to regulate many physiological processes, including reproduction, defensive responses, locomotor activity, glucose homeostasis, and appetite control (Canteras, 2002; King, 2006; Kow and Pfaff, 1998; Tong et al., 2007; Yokawa et al., 1989; Zhao et al., 2008). One of the earliest molecular markers expressed throughout the VMH is the nuclear receptor steroidogenic factor-1 (SF-1, NR5A1), which appears at embryonic (E) 9 (Ikeda et al., 2001). Although SF-1 is not required for the initial organization and migration of neurons to the developing VMH nucleus (Ikeda et al., 1995; Tran et al., 2003), this transcription factor is essential for terminal differentiation and maintenance of VMH neuronal populations (Davis et al., 2004; McClellan et al., 2006). Loss of SF-1 also results in diminished efferent projections to the amygdala (Tran et al., 2003) and altered afferent projections from the preoptic area to the VMH (Budefeld et al., 2011). Consistent with the essential role for SF-1 in the VMH, CNS-specific elimination of SF-1 in mice ($Sf\text{-}1^{Nestin:Cre}$) disrupts the integrity of the VMH and leads to a variety of metabolic, thermogenic, reproductive, and anxiety deficits (Kim et al., 2009, 2010, 2011; Zhao et al., 2008).

To delineate further the cellular and functional complexity of the VMH, several groups have exploited two *Sf1:Cre* driver transgenic mouse lines (Bingham et al., 2008; Dhillon et al., 2006) to ablate general factors known or thought to be associated with energy homeostasis. Indeed, increased susceptibility to diet-induced obesity has been reported for conditional knockouts of the leptin receptor (Bingham et al., 2008; Dhillon et al., 2006), insulin receptor (Klockener et al., 2011), phosphoinositol 3-kinase (PI3K; Xu et al., 2010), or SIRT1 deactylase (Ramadori et al., 2011) with the use of these *Sf1:Cre* drivers. Moreover, removing the central mediator of leptin resistance, Socs3, with the same *Sf1:Cre* driver, protects against diet-induced hyperglycemia (Zhang et al., 2008). More recently, a mild disturbance in energy balance in females was noted after the *Sf1:Cre* driver was used to eliminate conditionally the estrogen receptor α (ERα) from all SF-1-expressing tissues, including the ventrolateral region of the VMH (VMH_{vl}; Xu et al., 2011). Thus, these genetic lesions establish that disrupting cellular signaling in the VMH and its neuronal outputs (Klockener et al., 2011; Tong et al., 2007) alters normal energy homeostasis in mice.

Although these newer genetic approaches in mice have validated or refined the physiological roles of the VMH, the neuroanatomy of VMH projections in mice has yet to be described. Our current notion on how the VMH connects with other brain centers comes exclusively from stereotaxic injection studies with anterograde axonal tracers in adult rats (Canteras et al., 1994; Krieger et al., 1979; Saper et al., 1976). While results from these studies established projection patterns from different VMH subregions, the inherent

limitations of this method make it difficult to assess development of VMH projections during embryonic stages. Based on our earlier observations suggesting that the VMH and its projections are already established in neonatal mice (Kurrasch et al., 2007), two approaches that exploit the global expression of SF-1 in the VMH were used to trace the major VMH axonal projections during embryonic and postnatal stages. The first relied on tandem reporters, wheat germ agglutinin (WGA; Braz et al., 2002) and Tau-green fluorescent protein (TauGFP), knocked into the 3′-untranslated region (UTR) of the *Sf-1* (*Nr5a1*) locus. In this knock-in line, referred to as *Sf-1*^{TauGFP}, WGA and GFP are under the control of intact regulatory elements and are thus coexpressed and coregulated with SF-1 expression. In the second, more standard approach, the transgenic *Sf1:Cre* mouse was crossed with a *Z/EG* reporter mouse, resulting in constitutive expression of eGFP (enhanced GFP) after Cre-mediated recombination (Dhillon et al., 2006). This second reporter line, referred to as *Z/EG*$^{Sf1:Cre}$, expresses eGFP in all neurons derived from the SF-1 lineage, including cells that might no longer express *Sf-1*. By using both *Sf-1*^{TauGFP} and *Z/EG*$^{Sf1:Cre}$ mice, we show the temporal and anatomical patterns of VMH projections and show a marked difference in GFP labeling in the VMH_{vl} between these two lines.

MATERIALS AND METHODS

Generation of *Sf-1*^{TauGFP} line

The IRES-WGA-IRES-tauGFP knock-in targeting vector was created using 3.5-kb 5′ (657,441–653,959) and 2-kb (653,937–651,900) 3′ targeting arms that align with the endogenous *Sf-1* locus just after the stop codon in exon 7. The knock-in vector also included an ACN cassette (Bunting et al., 1999), which contains a loxP-flanked selectable marker *Neo*^{r} downstream of the testes-specific promoter from the angiotensin-converting enzyme gene used to drive expression of *Cre*. Thus, a self-induced deletion of the selectable marker occurred during passage through the male germline of mice. Southern blot analyses using a Neo-specific probe in *Sf-1*^{TauGFP} offspring confirmed complete elimination of the *Neo*^{r} gene from the *Sf-1* locus (data not shown). The gene encoding diphtheria toxin was also included outside the 3′ targeting arm for negative selection. Linearized targeting vector DNA was electroporated into E14Tg2A.4 (from 129/Ola mice) ES cells by the University of Michigan Transgenic Facility. ES clones were screened by using Southern blot analyses with both 5′ and 3′ probes. Positive clones were verified via PCR. Three positive clones were injected into 129-derived blastocysts and implanted into a pseudopregnant C57/Bl6 female. Offspring that were 70% chimeric or greater were then back-crossed to C57/Bl6 to confirm germline transmission

Animals

Mice were raised in our animal facility in strict accordance with a protocol approved by the UCSF Institutional Animal Care and Use Committee. All mice had ad libitum access to food and water. All *Sf-1*^{TauGFP} mice used in this study were homozygous as confirmed by PCR genotyping. For *Z/EG*$^{Sf1:Cre}$ mice, both the *Sf1:Cre* mice (line S7, generously provided by Dr. Elmquist) and the *Z/EG* line (provided by Dr. Pleasure, UCSF) were maintained as heterozygotes in a FVB/129 mixed background. *Sf-1*^{TauGFP} mice were maintained on a mixed 129/C56Bl6 mixed background. Embryos were collected at E10.5, E12.5, E14.5, and

E17.5 from timed-pregnant females (Tran et al., 2006) and from postnatal day (P) 0. Male mice were used for all studies.

Tissue collection and processing

Isolated embryos spanning stages E10.5–E14.5 were initially fixed in 4% paraformaldehyde (PFA) for 2 hours and equilibrated in 30% sucrose, followed by gross dissection of the upper body, which was equilibrated and mounted in OCT compound (Tissue-Tek, Torrance, CA). For E17.5 embryos, whole brains were removed, fixed in 4% PFA overnight, equilibrated in 30% sucrose, and mounted in OCT. P0 pups were perfused with phosphate-buffered saline (PBS) and 4% PFA as described previously (Kurrasch et al., 2007; Tran et al., 2003). Dissected brains were postfixed in 4% PFA for 2 hours, equilibrated in 30% sucrose, and mounted. All samples were sectioned at 20 μm.

Immunohistochemistry

Frozen brain sections (−80°C) were blown dry for 3 minutes and air dried at room temperature for 20 minutes. All steps described below were performed at room temperature, and washes were carried out for 3 × 5 minutes, unless otherwise noted. Sections were washed in a series of sequential buffers beginning with PBS (pH 7.5) and 0.3% Triton (PBST). This was followed by PBST and 0.3% hydrogen peroxide for 20 minutes and then PBST. Sections were transferred to a moistened incubation chamber (ThermoScientific, Fair Lawn, NJ), blocked with TNT blocking buffer (TNB; 1 M Tris-HCl pH 7.5, 0.15 M NaCl, 0.5% Blocking Reagent from PerkinElmer, Waltham, MA) for 1 hour, incubated with chicken anti-GFP antibody (1:2,500; Aves Labs, Tigard, OR) overnight at 4°C, and washed with TNT buffer (TNT; 0.1 M Tris-HCl, pH 7.5, 0.15 M NaCl, 0.05% Tween 20). Samples were then incubated with biotinylated anti-chicken antibody (1:500; Vector, Burlingame, CA) in TNT for 1 hour, washed in TNT, and incubated in streptavidin-HRP diluted in TNB (1:100; PerkinElmer) for 30 minutes. After TNT washes, samples were incubated with tyramide fluorescein diluted in amplification diluent (1:75; PerkinElmer) for 10 minutes and washed with TNT. Samples were equilibrated with a 5-minute wash (PBST), and incubated in 1× DAPI in PBST for 10 minutes. After the final washes in PBST, sections were mounted and cover-slipped with Fluoromount G (Southern Biotechnology, Birmingham, AL). Brains from the two mouse lines of the same developmental age were used in the same immunohistochemistry experiment. No-antibody controls were also performed.

For double-label experiments, perfused P0 tissues were used. Slides were washed in PBS and blocked for 1 hour (0.2% Triton and 10% donkey serum in 1× PBS). Tissues were incubated overnight with chicken anti-GFP (1:200; Aves Labs) and rabbit anti-SF-1 (1:100; Ingraham laboratory, UCSF) and washed with PBS and 0.3% Triton X. Samples were incubated with goat anti-chicken Alexa 488 (1:200; Invitrogen, Carlsbad, CA) and goat anti-rabbit Alexa 546 (1:200; Invitrogen) for 2 hours, washed in PBS with 0.3% Triton, and incubated with 1× DAPI for 10 minutes. Samples were washed in PBS for 10 minutes and then mounted in Fluoromount G. Sample size for all stages ranged between two and six per genotype.

Antibody characterization

See Table 1 for a list of all antibodies used in this study. The chicken anti-GFP antibody was generated against purified recombinant GFP emulsified in Freund's adjuvant and was analyzed by Western blot analysis (1:5,000 dilution) and immunohistochemistry (1:500 dilution) using transgenic mice expressing GFP gene product. No staining was seen in mice that lacked GFP.

The rabbit anti-SF-1 antibody was generated against purified recombinant SF-1 hinge LBD that spans amino acids 178–462 and was analyzed by Western blotting (1:1,000 dilution) with SF-1-positive and SF-1-negative cell lines. Signals were seen only in the SF-1-positive cell lines and not SF-1-negative cell lines. Immunostaining showed a pattern of cellular morphology and distribution in the mouse brain identical to that described in previous reports (Tran et al., 2006).

Histology

Histology was carried out on E17.5 and P0 brain sections rinsed in 95% ethanol for 15 minutes, 70% ethanol for 1 minute, and 50% ethanol for 1 minute. Sections were then washed in purified water twice for 2 minutes each and stained in cresyl violet for 5 minutes, followed by a brief rinse in purified water for 1 minute. Sections were destained in 50% ethanol for 1 minute and 70% ethanol with 1% glacial acetic acid for 2 minutes, followed by rehydration in 95% ethanol for 2 minutes and 100% ethanol for 1 minute. Sections were rinsed in xylene twice for 5 minutes each prior to coverslipping with Permount (Fisher Scientific, Pittsburgh, PA).

Image acquisition

All images were collected at the UCSF Nikon Imaging Center on a Nikon Ti high-throughput microscope (Nikon Instruments, Melville, NY). Fluorescent photomicrographs were taken with a CoolSnap HQ2 CCD camera (Photometrics, Roper Scientific, Tucson, AZ), and brightfield images were captured with a Nikon DS-Fi1 color camera and NIS-Elements software (Nikon Instruments). Photomicrographs were adjusted for contrast and brightness in Photoshop. Best attempts were made to determine anatomical identification and nomenclature using multiple references (Jacobowitz and Abbott, 1998; Paxinos, 2007; Schambra, 2008).

RESULTS

Generation and validity of the *Sf-1^{TauGFP}* reporter line

Sf-1^{TauGFP} mice were generated as described in Materials and Methods using the construct shown in Figure 1A. Immunohistochemistry directed against the wheat germ agglutinin (WGA) and TauGFP proteins revealed signals in all organs known to express SF-1, including the adrenal gland (Fig. 1B), gonads, and pituitary (data not shown). Although plant lectins such as WGA have been used successfully for transsynaptic neuronal tracing in some circumstances (Braz et al., 2002), very few efferent fibers were marked by WGA immunostaining in the *Sf-1^{TauGFP}* VMH. Expression of this plant lectin was limited to the soma and proximal neurites, with few if any signal observed in long axonal fibers, synaptic

terminals, or postsynaptic neurons (data not shown). Therefore, staining for WGA to map VMH projections was not pursued further. By contrast, detection of TauGFP protein by immunohistochemistry revealed a strong signal in the soma, with GFP colocalized with SF-1 and in neurites of VMH neurons (Fig. 1C–E). Thus, GFP was used to assess systematically SF-1 neuronal projections in embryonic and postnatal *Sf-1*^{TauGFP} mice. It should be noted that both Sf-1TauGFP male and female mice were viable and exhibited normal fertility.

Profile of GFP$^+$ neurons in *Sf-1*^{TauGFP} and *Z/EG*$^{Sf1:Cre}$ mice from E10.5 to E14.5

Beginning as early as E10.5, just prior to the onset of neurogenesis, GFP$^+$ cells are observed in the median eminence (ME) of *Sf-1*^{TauGFP} mice (Fig. 2A), with fibers extending into the medial forebrain bundle (MFB; Fig. 2C) and traveling toward the epithalamus. At this stage, expression in *Z/EG*$^{Sf1:Cre}$ mice was nearly undetectable, with only sparse GFP$^+$ cells present (Fig. 2B,D). However, in slightly older embryos, at E12.5, GFP$^+$ cells were observed in the ME (Fig. 3A,B) and in the caudal, lateral postoptic area or presumptive VMH in both *Sf-1*^{TauGFP} and *Z/EG*$^{Sf1:Cre}$ mice (Fig. 3C–F), with GFP$^+$ neurons occupying the lateral half of the hypothalamus and extending to the edge of the developing brain (Fig. 3E,F). Fiber strands that travel through the MFB are easily observed in *Sf-1*^{TauGFP} (Fig. 3A,C) but are faintly visible in *Z/EG*$^{Sf1:Cre}$ (Fig. 3B,D). The most dominant fiber tract visible in *Sf-1*^{TauGFP} mice travels medial to the optic tract and lateral to the MFB, following a path similar to the presumptive ventral supraoptic commissure (vSOC; Fig. 3C) as previously reported for adult rats (Canteras et al., 1994).

Later in neurogenesis (E14.5), *Sf-1*^{TauGFP} and *Z/EG*$^{Sf1:Cre}$ GFP$^+$ cells begin to appear anterior to the ME (Fig. 4A,B) and in the coalescing VMH, which is bounded medially by the ventricular wall and laterally by the developing diencephalon (Fig. 4C,D). At this stage, striking differences between the *Sf-1*^{TauGFP} and *Z/EG*$^{Sf1:Cre}$ mice are observed in the most lateral aspect of the presumptive VMH (Fig. 4E–H). Notably, an absence of GFP$^+$ cells is observed in this VMH$_{vl}$ region in *Sf-1*^{TauGFP} mice (Fig. 4E,G). With respect to the vSOC tract, both reporter lines exhibit fibers that initially travel on a ventral anterior course, with some reaching the level of the suprachiasmatic nucleus (SCN), before moving laterally in a ventral and posterior direction. Most of these fibers travel along the lateral wall of the developing brain and branch toward the epithalamus (Fig. 4E,F) and the habenular nucleus. Few if any fibers reach the level of the periaqueductal gray (PAG; data not shown). A second, scattered group of fibers traverse through the MFB, ascending laterally and dorsolaterally in a fan-like pattern (Fig. 4C,D). These fibers likely originate from neurons located either in the anterior or in the anteriolateral aspect of the VMH. Although some of these fibers join the vSOC at the level of the external medullary lamina (EML), others spread into the thalamus extending beyond the EML (Fig. 4E,G). Few if any fibers travel medially in the periventricular zone (Fig. 4E–H).

Collectively, data obtained with the *Sf-1*^{TauGFP} reporter line establish that VMH projections begin as early as E10.5, just at the onset of the window of VMH neurogenesis (E10.5–E15.5). Despite the fact that GFP expression was observed to lag in *Z/EG*$^{Sf1:Cre}$ brains, the intensity and pattern of labeling and the appearance of projections are roughly equivalent in both lines by E14.5. However, labeling in the VMH$_{vl}$ was markedly different. Whereas the

number and pattern of GFP^+ neurons is far greater and broader, respectively in *Z/EG*$^{Sf1:Cre}$ mice (Fig. 4F), a much more restricted and medial pattern with fewer positive cells is observed in *Sf-1*^{TauGFP} mice (Fig. 4E). Given that the SF-1 lineage is marked by *Sf1:Cre*-mediated recombination, we infer that SF-1 is only transiently expressed in neurons that migrate and populate the VMH_{vl}.

Prenatal ascending and descending SF-1 tracts at E17.5

The intensities of VMH projections in *Sf-1*^{TauGFP} and *Z/EG*$^{Sf1:Cre}$ mice begin to differ at E17.5. Whereas the ascending projections are observed in *Z/EG*$^{Sf1:Cre}$ mice, including those originating from the retrochiasmatic area (RCh) and traveling to the medial basal forebrain (Fig. 5A–C), these fiber tracts are less intense in *Sf-1*^{TauGFP} mice (data not shown). The first ascending fiber tract, which is far brighter in *Z/EG*$^{Sf1:Cre}$ mice, travels through the medial aspect of the hypothalamus and reaches the medial basal forebrain (Figs. 5A–C, 6A–D). Fibers were found in the RCh (Fig. 6C,D), the anterior hypothalamic area (Fig. 6A,B), and medial preoptic area (MPoA) but not in the lateral preoptic area (LPoA) or in the SCN (Fig. 6B,C). Other fibers were observed to turn ventrolaterally, traveling along the EML toward the bed nucleus of stria terminalis (BNST) or terminating in the BNST at the level of the anterior commissure (Fig. 5B,C). Moving anteriorly, positive fibers were detected in the diagonal and vertical band of Broca as well as in the medial septum (Fig. 5A).

The second group of fibers innervating targets anterior to the VMH travels along the base of the brain (Fig. 6A–D), follows the midline circumventing the RCh, and stays ventral to the SCN. At the posterior part of the SCN, some fibers travel medially along the ventricular wall to reach the paraventricular hypothalamic nucleus (PVH; Fig. 6A,B). Fibers in this tract show intense GFP labeling and are thus presumably tightly packed. At the level of the SCN, this tract begins to move laterally along the base of the brain, gradually turning caudally while continuing to ascend dorsally to form the brightly labeled vSOC tract (Fig. 6A–D). Throughout the anterior VMH, there are fibers that emerge from the ventral–lateral aspect of the nucleus to join directly with the vSOC (Fig. 6C,D).

Three major pathways constitute VMH projections to caudal regions of the brain. As with the ascending tracts, the intensity of these descending tracts appears brighter in *Z/EG*$^{Sf1:Cre}$ mice. The first pathway begins by following the vSOC anterior along the base of the brain and then curves on a rostral–ventral path before arcing back in a caudal–ventral path (Fig. 6C,D). The C-shaped course is similar to that of efferent fibers that innervate the hypothalamus, such as the fornix and the stria medullaris. This tightly bundled tract disperses at the lateral aspect of the medial lemniscus, sending parallel branches through the thalamus along the EML (Fig. 6C,D). Many of these vSOC fibers traverse through the posterior thalamic nucleus, lateral posterior thalamic nucleus, and lateral dorsal nucleus and terminate in the habenular nucleus (Fig. 6C,D). More caudally, vSOC fibers course through the medial geniculate body (Fig. 6E–H).

The second descending pathway travels along the zona incerta (Fig. 6E–H). Many of these fibers emerge from the dorsal–lateral aspect of the nucleus and travel parallel to the vSOC at the lateral aspect of the medial lemniscus. Small numbers of fibers located more ventrally

arc back across the internal capsule to join together with branches from the vSOC (Fig. 6E–H).

The third descending tract innervates midline structures in the posterior diencephalon and the midbrain (Fig. 6E–H). This tract originates from the posterior aspect of the VMH and follows the periventricular system extending along the midline of the brain to traverse through the dorsomedial nucleus and posterior hypothalamus (Fig. 6I,J) to reach the PAG region. Indeed, the entire PAG is decorated with intense GFP^+ fibers (Fig. 6I–L).

At this late embryonic stage, the vSOC remains the major fiber tract in both mouse models, whereas other ascending and descending SF-1 tracts begin to mature and are generally brighter in *Z/EG*$^{Sf1:Cre}$ mice. Furthermore, the aforementioned absence of GFP labeling in the *Sf-1*^{TauGFP} VMH_{vl} region becomes more evident at E17.5 (Fig. 6E–J), especially in the region lateral to the fornix. In stark contrast, GFP^+ cells in the *Z/EG*$^{Sf1:Cre}$ VMH_{vl} extend beyond the VMH proper to the lateral border of the hypothalamus (Fig. 6E–J).

Neonatal ascending and descending SF-1 tracts in *Sf-1*^{TauGFP} mouse at P0

We next examined ascending and descending fibers in neonatal mice at P0. At this stage, *Sf-1*^{TauGFP} mice show projection patterns similar to those of *Z/EG*$^{Sf1:Cre}$ mice (Fig. 7A–D), except for the sparse GFP^+ cells observed in the midbrain of *Z/EG*$^{Sf1:Cre}$ mice (Fig. 7E,F). In addition, and similar to earlier developmental stages, GFP^+ neurons are undetectable in the *Sf-1*^{TauGFP} VMH_{vl} region (Fig. 7G,H). To show that this absence truly reflects a loss of SF-1 in the VMH_{vl} region, double labeling was carried out in both the *Sf-1*^{TauGFP} and the *Z/EG*$^{Sf1:Cre}$ lines. As expected, GFP^+ cells in the *Sf-1*^{TauGFP} line colabeled with SF-1-positive neurons, with a notable absence of both signals in the VMH_{vl} region (Fig. 7I,K,L). In contrast, GFP^+ cells that no longer express SF-1 continue to be present in the VMH_{vl} region (Fig. 7J,M,N). Taken together, these data suggest that neurons in this VMH subregion adopt a different cell fate from the rest of the VMH.

To describe projection patterns at a later stage, we used the *Z/EG*$^{Sf1:Cre}$ line, which exhibited well-defined and visible VMH projections (Fig. 8A–R). Two ascending tracts innervate the anterior limbic system and the medial basal forebrain. Ascending fibers project anteriorly through the RCh and begin the lateral branching of the vSOC by traveling dorsally to the optic tract. Heavy innervation of the entopenducular nucleus by the vSOC is observed (Fig. 8D). Furthermore, multiple branches emerge from the vSOC to innervate the medial division of the central amygdaloid nucleus (Fig. 8D,E,S–U) and, to a lesser extent, the anterodorsal part of the medial amygdaloid nucleus. These fibers travel caudally to innervate the remaining divisions of the central amygdaloid nucleus, including the lateral division and the capsular part. The posterodorsal medial amygdaloid nucleus also receives some fiber projections. Few fibers if any were observed in other regions of the amygdala (data not shown).

The anterior hypothalamus and the medial basal forebrain received the strongest ascending innervations from the VMH, with fibers traveling through the periventricular zone, the medial zone of the hypothalamus, and some possibly through the medial forebrain bundle. Dense fibers are found in the anterior hypothalamic area, the PVH, and the perifornical

region (Fig. 8C,D). In contrast, the lateral hypothalamus is devoid of fibers. As noted at earlier stages, fibers surround, but do not directly innervate, the SCN (Fig. 8C). Rostrally, both the medial and the lateral parts of the medial preoptic nucleus, as well as the MPoA, are covered with fibers. Few fibers are found in the anteroventral periventricular nucleus and the LPoA (Fig. 8B). Fibers in the medial hypothalamus ascend to innervate heavily the BNST, spanning laterally to medially (Fig. 8A,B). Other fibers travel medially to innervate the thalamus, densely in the anteromedial nucleus and moderately in the paraventricular thalamic nucleus and anteroventral and anterodorsal thalamic nuclei. At the level where the anterior commissures join, intense fiber tracts are observed in the septohypothalamic nucleus, the BNST, and the lateral septal nucleus (Fig. 8A).

Three descending fiber tracts observed at E17.5 persist at P0: the vSOC, the zona incerta, and the periventricular system. These fibers begin as distinct tracts but join together distal to the VMH. The periventricular system emanates from the posterior aspect of the VMH and innervates the dorsal premammillary nucleus (Fig. 8H) and, to a lesser extent, the ventral premammillary nucleus (Fig. 8G–I). These fibers travel through the mammillary nucleus while staying medial to the mammilotegmental tract and the fasciculus retroflexus. They course through the posterior hypothalamic nucleus (Fig. 8H) and the precommissural nucleus (Fig. 8H) to reach the PAG. Upon reaching the PAG, these fibers merge with fibers from the dorsal arm of the vSOC (Fig. 8F–I).

The descending vSOC tract consists of fibers that emerge from the anterior part of the VMH, including cells in the RCh (Fig. 8D). The fiber bundle moves dorsally and gives off lateral branches that contribute to the amygdaloid complex (see above). The vSOC consists of mostly efferent fibers that emerge from the anterior half of the VMH and travel dorsally to the optic tract as a tightly bundled tract before turning medially at the lateral aspect of the medial leminiscus (Fig. 8D–F). After the turn, fibers in the vSOC follow the path of the EML through the thalamus to reach the habenular nucleus anteriorly (Fig. 8C,D) and the PAG posteriorly.

The zone incerta tract is a group of loosely bundled fibers emerging from the dorsal and dorsolateral aspects of the VMH (Fig. 8E,F). This fiber tract courses through the general area of the zona incerta and merges with the vSOC at approximately the lateral aspect of the medial lemniscus, medial to the ventral geniculate nucleus. Fiber density is extremely high at the level of the merger, which encompasses the subgeniculate nucleus, the epipenducular nucleus, the peripenducular nucleus, and the lateral terminal nucleus of the accessory optic tract (Fig. 8F,G). These fibers then fan out, with the majority traveling around it and coursing through the subbrachial nucleus, the posterior intralaminar thalamic nucleus, and the posterior thalamic nucleus; a few enter the medial geniculate nucleus (Fig. 8H–J). Some fibers enter the deep layer of the superior colliculus, but most travel toward the PAG (Fig. 8G–J). Notably, some fibers that travel in the zona incerta pathway appear to course ventrally in parallel to the periventricular system and generally proceed toward the dorsal end of the vSOC or directly to the PAG.

Although these three fiber tracts travel in distinct courses, they initially send branches that merge with each other, forming an intercalating network. Joining vSOC that courses through

the thalamus are branches that emerge from the periventricular system (Fig. 8D–H). These fibers travel laterally, just ventral to the fasciculus retroflexus, to reach its lateral target of the ventral geniculate nucleus. At that point, they merge with the fibers from the vSOC as well as those from the zona incerta pathway. As these fibers course transversely across the brain, they intersect almost perpendicularly with fibers that come from the zone incerta that travel parallel to the periventricular system (Fig. 8H).

Fibers from the vSOC and the periventricular system meet at the PAG and travel along the aqueduct and innervate the rostrocaudal axis of the PAG (Fig. 8I–R). Dense fibers were also found in the deep layer of the superior colliculus (Fig. 8I–L) and the subbrachial nucleus (Fig. 8J–L). Moderate to dense fibers could also be seen in the mesencephalic reticular formation (Fig. 8K,L) and the ventral tegmental area (Fig. 8K) but not in the red nucleus or substantia nigra. Moving caudally, moderate fibers are seen throughout the tegmental nucleus, laterodorsal tegmental nucleus (Fig. 8M–O), and lateral parabrahchial nucleus (Fig. 8N,O). In the pons, the locus coeruleus receives fiber projections (Fig. 8P), but very few fibers are found in the pontine reticular area. The lateral tegmental nucleus and the dorsal raphe nucleus appear to be completely devoid of fibers. Taken together, the neonatal VMH projections at P0 extend to broad regions of the brain, including the anterior hypothalamus, the amygdala, discrete hypothalamic and thalamic nuclei, the rostrocaudal axis of the PAG, and sparse nuclei in the brainstem.

DISCUSSION

By using two distinct, but complementary, genetic tracing approaches, we have analyzed the development of VMH efferent projections, as marked by SF-1. The vSOC tract is the first of five major pathways to develop and can be observed prominently as early as E10.5, just 1 day after SF-1 is expressed in postmitotic neurons. Moreover, although VMH projections are conserved in mice and rats, as expected, we found that efferent projection patterns at early developmental stages are remarkably similar to adult patterns (Fig. 9). Although it has been generally assumed that SF-1 marks the entire VMH because of its early and broad expression, the striking differences observed in GFP^+ labeling between the $Sf\text{-}1^{TauGFP}$ and the $Z/EG^{Sf1:Cre}$ lines imply that SF-1 is transiently expressed at early embryonic stages and then silenced in neurons that populate the VMH_{vl}. Thus, with the one exception of the VMH_{vl}, the *Sf1:Cre* driver faithfully recapitulates SF-1 expression in the brain. These findings also suggest the female-specific traits classically associated with the VMH_{vl} are mediated by distinct SF-1-negative neurons.

Developmental profiles of SF-1 neuronal projections

VMH neurons are born in the ventricular zone between E10 and E15 (Shimada and Nakamura, 1973; Tobet et al., 1999) and migrate radially to their final destination. SF-1 neurons share a similar developmental pattern in that they are born between E9.5 and E15.5 in mice, peaking at E13.5 (Ikeda et al., 1995, 2001; Tran et al., 2003). Formation of the VMH nuclei occurs later, at E15–E17 (Tobet et al., 1999). Both mouse models used in our study show SF-1 neurons in the presumptive VMH area by E10.5. However, these neurons begin to coalesce into the conventional oval nucleus only later in development at E14.5.

Regardless of whether SF-1 neurons are marked by the endogenous SF-1 promoter or by Cre recombination, the overall projection patterns and final target sites appear invariable. The most prominent embryonic fiber tract is the presumptive vSOC, which travels through the dorsal thalamus and targets the PAG. Clearly, further work is needed to assess the functional significance, of these early embryonic VMH projections.

Comparison of the timing and expression patterns between the *Sf-1*^{TauGFP} and the *Z/EG*$^{Sf1:Cre}$ mice establish that anatomical divisions within the VMH begin early in development. One of the most striking differences noted between these two reporter mice was the presence or absence of GFP labeling in the VMH_{vl} (Table 2). Indeed, although SF-1 staining has been used to define the VMH in rodents (Dellovade et al., 2000; Shinoda et al., 1995), our collective results show that the lateral boundary of the VMH, as defined by the *Z/EG*$^{Sf1:Cre}$ line, extends well beyond SF-1 staining and the Nissl-stained VMH cluster. These data imply that, although the VMH_{vl} shares a common SF-1 lineage with other VMH subregions, developmental signals must begin to silence SF-1 expression in the VMH_{vl} prior to E14.5. That VMH_{vl} has a unique molecular signature fits well with the specialized function of the VMH_{vl} in female reproduction and energy expenditure. Indeed, expression of steroid nuclear receptors, ERα and progesterone receptors (Hagihara et al., 1992; Simerly et al., 1990), and the homeobox transcription factor Nkx2-1 is highly restricted to the VMH_{vl} (Davis et al., 2004; Tran et al., 2003). Our findings also underscore the need for careful design when using an *Sf1:Cre* strategy to ablate genes in the VMH.

Timing of expression patterns was also different between *Sf-1*^{TauGFP} and *Z/EG*$^{Sf1:Cre}$ mice (Table 2). Both models show distinct GFP^+ cells in the ME and the presumptive VMH between E10.5 and E12.5, but the numbers are generally higher in the *Sf-1*^{TauGFP} model. Fiber tracts are poorly developed in *Z/EG*$^{Sf1:Cre}$ mice at E10.5 but prominent in *Sf-1*^{TauGFP} mice. By E14.5, *Z/EG*$^{Sf1:Cre}$ mice “catch up” and exhibit identical fiber tracts with equivalent intensities as observed in *Sf-1*^{TauGFP} mice. This lag in GFP expression is consistent with the well documented delay in Cre-recombinase activity observed in many Cre lines (Nagy, 2000). By contrast, the fidelity of GFP expression is maintained in the knock-in *Sf-1*^{TauGFP} reporter and is easily observed at E10.5. At older stages, the situation is reversed, with the *Z/EG*$^{Sf1:Cre}$ showing a much more intense pattern of GFP labeling than that observed in the *Sf-1*^{TauGFP} knock-in reporter line. We attribute this weakening of postnatal GFP labeling to declining *Sf-1* transcripts, as observed in neonatal mice (Kurrasch et al., 2007). This factor coupled with the positioning of the *TauGFP* gene downstream of the second IRES would exacerbate this postnatal drop in *Sf-1* transcripts. Notably, other than the VMH_{vl}, only a few GFP^+ neurons were detected in extra-VMH sites in *Z/EG*$^{Sf1:Cre}$ brain regions, specifically the brainstem. Thus, unlike the case in other Cre lines, including the hypothalamic *Pomc:Cre* line (Morrison and Munzberg, 2012; Padilla et al., 2010, 2012), appropriate regulatory elements of SF-1 transcription are present in the $^{Sf1:Cre}$ transgene, confirming the anatomical reliability of this line (Dhillon et al., 2006).

VMH ascending and descending projections

Efferent VMH projections described here in neonatal mice show remarkable similarity to those described previously for adult rats using stereotaxic injections (Canteras et al., 1994;

Krieger et al., 1979; Saper et al., 1976). Efferent projections of SF-1 neurons can be divided into either 1) ascending tracts that innervate structures anterior to the nucleus in the hypothalamus, the basal forebrain, and the telencephalon or 2) descending tracts that innervate structures dorsal and posterior to the nucleus in the caudal hypothalamus, the thalamus, and the brainstem. Both the *Sf-1*^{TauGFP} and the *Z/EG*$^{Sf1:Cre}$ mice exhibit SF-1 efferent fibers that project to perifornical area and the PVH. Many of these fibers appear to originate from GFP^{+} cells in the RCh area as well as the very anterior aspect of the VMH. Although fibers from the medial zone of the hypothalamus projecting to the PVH, as proposed in an adult rat study (Canteras et al., 1994), are easily observed here by genetic tracing, nongenetic tracing methods have generally missed these tracts because of their near-midline location (Krieger et al., 1979; Saper et al., 1976).

In both *Sf-1*^{TauGFP} and *Z/EG*$^{Sf1:Cre}$ mice, the anterior hypothalamic area receives abundant projections from GFP^{+} neurons via the medial hypothalamic zone and the medial forebrain bundle, consistent with known VMH inputs into those areas (Canteras et al., 1994; Conrad and Pfaff, 1976; Krieger et al., 1979; Risold et al., 1994; Saper et al., 1976). Many GFP-labeled sites within the anterior hypothalamic area and forebrain are involved in the regulation of reproductive behavior and are known to be sexually dimorphic. Consistent with studies in rats (Canteras et al., 1994), the MPoA and the medial preoptic nucleus were both found to receive the majority of these innervations, whereas the LPoA was devoid of any GFP label. Most of these ascending fibers likely originate from the VMH$_{vl}$ (Canteras et al., 1994), supporting the prominent role of this VMH subregion in female reproductive physiology (Hagihara et al., 1992; Simerly et al., 1990). The BNST is another sexually dimorphic brain region that is innervated by the VMH. Indeed, our data show that fiber tracts course dorsally to terminate in a broad region within the BNST, which matches the pattern in adult mouse (Tong et al., 2007) as well as in the rat (Canteras et al., 1994; Krieger et al., 1979; Saper et al., 1976).

Several structures of the limbic system receive significant GFP^{+} innervation. The sexually dimorphic septal nuclei receive differential innervation with the lateral septal nucleus, receiving significantly more GFP^{+} fibers than the medial septal nucleus. Although the degrees of innervation to the lateral septal nucleus and to the BNST are comparable in mice, the lateral septal nuclei was found to receive significantly less innervation than the BNST in rats (Canteras et al., 1994). Another major limbic structure that receives VMH innervation is the amygdala. GFP^{+} fibers reach the amygdala in the mouse almost exclusively through the vSOC tract, specifically from branches of the vSOC that are traveling anterodorsally before arching back to course caudally toward the PAG. In contrast, VMH projections to the amygdala in the rat consist of ansa peduncularis fibers found in the vSOC and fibers that travel through the substantia innominata (Canteras et al., 1994). In addition, although many different regions in the amygdala receive significant input from the VMH in adult rats, our studies in mice show that the central amygdaloid nucleus receives the majority of the input.

Descending VMH efferents in the mouse share many similar targets with those in the rat, although mild differences are noted as well. Some periventricular fibers initially travel sparsely through other hypothalamic regions, but we were unable to detect prominent projections to the premammillary nucleus as previously reported (Canteras et al., 1994).

Perhaps in the rat these fibers originate from the anterior hypothalamic nucleus, which is in close proximity to the anterior VMH (Risold et al., 1994). Both rats and mice harbor projections to the posterior hypothalamic nucleus with fibers that originate from the dorsal aspect of the VMH and travel through the zona incerta to the vSOC (Canteras et al., 1994). We also found that, as reported by others for the rat, the PAG receives the largest amount of fibers from the VMH, primarily through the midbrain periventricular system and vSOC (Canteras et al., 1994; Krieger et al., 1979; Saper et al., 1976). Furthermore, we confirm that brainstem structures such as the deep layer of the superior colliculus, the mesencehpalic reticular formation, the subbrachial nucleus, and the locus coeruleus all appear to receive VMH innervations in both the rat and the mouse (Canteras et al., 1994; Krieger et al., 1979).

Functional implications of SF-1 projections in VMH physiology in the mouse

Having mapped embryonic and postnatal VMH projections in mice, we can now ask how these different fiber tracts might be related to the known adult physiological functions of the VMH, including metabolism, defensive behavior, and female reproduction. From our data, we suggest that SF-1 neurons targeting the general vicinity of gonadotropin-releasing hormone (GnRH) neurons, including the medial POA and the diagonal band of Broca, have the potential to modulate expression and/or secretion of GnRH. Abnormal regulation of these neurons might underlie the abnormal estrous cycle and infertility observed in *Sf-1*$^{Nestin:Cre}$ female mice (Ikeda et al., 1995; Kim et al., 2010). In addition, intense projections to the PAG are also predicted to impact female reproductive behavior. In this regard, a recent study in female rats shows that the VMH_{vl} is important for maternal care (Cameron et al., 2011) and that siRNA interference of ERa in the VMH_{vl} results in increased aggression against juvenile rats (Musatov et al., 2006).

Significant inputs from the VMH to the septal nucleus, anterior hypothalamic nucleus, dorsal premammillary nucleus, and extrahypothalamic regions such as PAG are also predicted to mediate anxiety and defensive behaviors that have been linked to the VMH (Canteras, 2002). Indeed, *Sf-1*$^{Nestin:Cre}$ mice exhibit increased anxiety (Kim et al., 2009).

The VMH also plays an important role in metabolism (King, 2006; Lopez et al., 2010; Yi et al., 2011) that is likely mediated by SF-1 neurons. Although the *Sf-1*$^{Nestin:Cre}$ mice fail to exhibit an obvious metabolic phenotype, several mouse models show altered metabolism when components of the leptin signaling pathway are ablated in SF-1-expressing cells (Bingham et al., 2008; Dhillon et al., 2006; Xu et al., 2010; Zhang et al., 2008). With the assumption that these metabolic defects arise from central loss of SF-1 rather than peripheral ablation of these genes in gonads, adrenals, or the anterior pituitary, these collective metabolic phenotypes underscore the importance of SF-1 neurons in energy homeostasis. Consistent with these studies, SF-1 neurons project to areas implicated in body weight regulation, including the PVH. In contrast to an earlier study indicating that VMH neurons make synaptic contacts with ARC neurons (Sternson et al., 2005), we were unable to detect any GFP^+ fibers within the ARC. It remains possible that synaptic connections between the VMH and the ARC occur on the shell of the VMH (Fu and van den Pol, 2008; Millhouse, 1973) or that SF-1-negative neurons innervate the ARC. The VMH also affects glucose homeostasis via direct or indirect innervation to the autonomic nervous system. A

conditional knockout of vesicular glutamate transporter 2 (*Vglut2*$^{Sf1:Cre}$) exhibited a blunted response to hypoglycemia, with a diminished release in glucagon. The dorsal motor nucleus of the vagus (DMV) is proposed to mediate this VMH function. (Tong et al., 2007). Although it has been suggested that DMV may receive neuronal projections from the VMH (Lopez et al., 2010), our study and other studies failed to detect any direct SF-1 or VMH projections to the DMV (Canteras et al., 1994; Tong et al., 2007).

Future molecular and genetic dissection of the VMH will surely provide insight into how this complex hypothalamic nucleus integrates emotional responses with metabolism and reproduction. We predict, based on the extensive VMH projections previously defined in rats, and now here in mice, that the VMH will influence other physiological functions. For instance, the strong VMH projections to areas surrounding the SCN could very well account for the diurnal rhythm of corticosterone release previously attributed to the VMH (Choi et al., 1998). In addition, efferent projections to the subthalamic locomotor region suggest that the VMH is involved in locomotor activity (Narita et al., 1998; Yokawa et al., 1989). Finally, the intense VMH projections to the central and medial amygdaloid nuclei are likely to mediate emotional processing.

In summary, our genetic tracing studies show that VMH efferent projections are established early in the embryo and are conserved in rodents. We also find that the VMH_{vl} develops into a discrete region that extends well beyond the classical morphological boundary of the VMH. Thus, our results challenge the traditional anatomical definition of the VMH and underscore the regional complexity of a hypothalamic nucleus.

Acknowledgments

Grant sponsor: National Institute of Diabetes and Digestive and Kidney Diseases; Grant number: R01DK063592 (to H.A.I.); Grant sponsor: Lawson Wilkins Pediatric Endocrine Society (to C.C.C.); Grant sponsor: National Institute of Diabetes and Digestive and Kidney Diseases; Grant number: 1K08DK076721 (to C.C.C.); Grant sponsor: Giannini Postdoctoral Fellowship (to D.M.K.).

We thank Drs. A. Basbaum, N. Shah, and M. Capecchi for reagents used in building the construct for the *Sf-1*^{TauGFP} mouse line. We especially thank Drs. J.L.R. Rubenstein, G. Lee, S. Correa, and E. Faivre for guidance on and discussion of this article. We also thank D. Newstrom for technical assistance. Data were acquired from the Nikon Imaging Center at UCSF/QB3.

Abbreviations

12N	hypoglossal nucleus
3N	oculomotor nucleus
3V	third ventricle
4N	trochlear nucleus
4V	fourth ventricle
5N	motor trigeminal nucleus
ac	anterior commissure
AD	anterodorsal nucleus of the thalamus

AH	anterior hypothalamic area
AM	anteromedial nucleus of the thalamus
APT	anterior pretectal nucleus
Aq	aqueduct
Arc	arcuate nucleus
AV	anteroventral nucleus of the thalamus
bic	brachium of the inferior colliculus
BM	basomedial amygdaloid nucleus
BNST	bed nucleus of stria terminali
CeA	central amygdaloid nucleus
CG	central gray
CN	cuneiform nucleus
DLG	dorsal lateral geniculate nucleus
DMH	dorsomedial nucleus of the hypothalamus
DR	dorsal raphe nucleus
eml	external medullary lamina
EP	entopenduncular nucleus
f	fornix
fr	fasicuculus retroflexus
ic	internal capsule
IC	inferior colliculus
IP	interpeduncular nucleus
LC	locus coeruleus
LD	lateral dorsal nucleus of the thalamus
LDTg	lateral dorsal tegmental nucleus
LHA	lateral hypothalamic area
LHb	lateral habenular nucleus
LM	lateral mammillary nucleus
LP	lateral posterior nucleus of the thalamus
LPB	lateral parabrachial nucleus
LPoA	lateral preoptic area
LS	lateral septal nucleus

MeA	medial amygdaloid nucleus
Me5N	mesencephalic trigeminal nucleus
MG	medial geniculate nucleus
MHb	medial habenular nucleus
ml	medial lemniscus
mlf	medial longitudinal fasciculus
MM	medial mammillary nucleus
MPoA	medial preoptic area
MS	medial septal nucleus
mt	mammillothalamic tract
MVeN	medial vestibular nucleus
ND	nucleus of Darkschewitsch
ot	optic tract
PAG	periaqueductal gray
pc	posterior commissure
PF	parafasicular nucleus (F)
PH	posterior hypothalamic nucleus
PMD	premammillary nucleus, dorsal part
PMnR	paramedian raphe nucleus
PMV	permammillary nucleus, ventral part
PN	pontine nucleus
PrC	precommissural nucleus
PVA	paraventricular nucleus of the thalamus, anterior part
PVH	paraventricular nucleus of the hypothalamus
PVT	paraventricular nucleus of the thalamus
R	red nucleus
Re	nucleus reuniens
RF	reticular formation, midbrain
Rt	reticular nucleus of the thalamius
SC	superior colliculus
SCN	suprachiasmatic nucleus
sm	stria medullaris

SN	substantia nigra
SNr	substantia nigra, reticular part
Sol	neuclus of the solitary tract
st	stria terminalis
STN	subthalamic nucleus
SubB	subbrachial nucleus
SubG	subgeniculate nucleus
TgN	tegmental nucleus
VG	ventral geniculate nucleus
VL	ventrolateral nucleus of the thalamus
VM	ventromedial nucleus of the thalamus
VMH	ventromedial nucleus of the hypothalamus
VMPO	ventromedial preoptic nucleus
VPL	ventral posterolateral nucleus
VPM	ventral posteromedial nucleus
vsoc	ventral supraoptic commissure
VTA	ventral tegmental area
ZI	zona incerta

LITERATURE CITED

Bingham NC, Anderson KK, Reuter AL, Stallings NR, Parker KL. Selective loss of leptin receptors in the ventro-medial hypothalamic nucleus results in increased adiposity and a metabolic syndrome. Endocrinology. 2008; 149:2138–2148. [PubMed: 18258679]

Braz JM, Rico B, Basbaum AI. Transneuronal tracing of diverse CNS circuits by Cre-mediated induction of wheat germ agglutinin in transgenic mice. Proc Natl Acad Sci U S A. 2002; 99:15148–15153. [PubMed: 12391304]

Budefeld T, Tobet SA, Majdic G. Altered position of cell bodies and fibers in the ventromedial region in SF-1 knockout mice. Exp Neurol. 2011; 232:176–184. [PubMed: 21906594]

Bunting M, Bernstein KE, Greer JM, Capecchi MR, Thomas KR. Targeting genes for self-excision in the germ line. Genes Dev. 1999; 13:1524–1528. [PubMed: 10385621]

Cameron NM, Soehngen E, Meaney MJ. Variation in maternal care influences ventromedial hypothalamus activation in the rat. J Neuroendocrinol. 2011; 23:393–400. [PubMed: 21418337]

Canteras NS. The medial hypothalamic defensive system: hodological organization and functional implications. Pharmacol Biochem Behav. 2002; 71:481–491. [PubMed: 11830182]

Canteras NS, Simerly RB, Swanson LW. Organization of projections from the ventromedial nucleus of the hypothalamus: a *Phaseolus vulgaris*-leucoagglutinin study in the rat. J Comp Neurol. 1994; 348:41–79. [PubMed: 7814684]

Choi S, Wong LS, Yamat C, Dallman MF. Hypothalamic ventromedial nuclei amplify circadian rhythms: do they contain a food-entrained endogenous oscillator? J Neurosci. 1998; 18:3843–3852. [PubMed: 9570813]

Conrad LC, Pfaff DW. Efferents from medial basal forebrain and hypothalamus in the rat. II. An autoradiographic study of the anterior hypothalamus. J Comp Neurol. 1976; 169:221–261. [PubMed: 61213]

Davis AM, Seney ML, Stallings NR, Zhao L, Parker KL, Tobet SA. Loss of steroidogenic factor 1 alters cellular topography in the mouse ventromedial nucleus of the hypothalamus. J Neurobiol. 2004; 60:424–436. [PubMed: 15307147]

Dellovade TL, Young M, Ross EP, Henderson R, Caron K, Parker K, Tobet SA. Disruption of the gene encoding SF-1 alters the distribution of hypothalamic neuronal phenotypes. J Comp Neurol. 2000; 423:579–589. [PubMed: 10880989]

Dhillon H, Zigman JM, Ye C, Lee CE, McGovern RA, Tang V, Kenny CD, Christiansen LM, White RD, Edelstein EA, Coppari R, Balthasar N, Cowley MA, Chua S Jr, Elmquist JK, Lowell BB. Leptin directly activates SF1 neurons in the VMH, and this action by leptin is required for normal body-weight homeostasis. Neuron. 2006; 49:191–203. [PubMed: 16423694]

Fu LY, van den Pol AN. Agouti-related peptide and MC3/4 receptor agonists both inhibit excitatory hypothalamic ventromedial nucleus neurons. J Neurosci. 2008; 28:5433–5449. [PubMed: 18495877]

Hagihara K, Hirata S, Osada T, Hirai M, Kato J. Distribution of cells containing progesterone receptor mRNA in the female rat di- and telencephalon: an in situ hybridization study. Brain Res Mol Brain Res. 1992; 14:239–249. [PubMed: 1331652]

Ikeda Y, Luo X, Abbud R, Nilson JH, Parker KL. The nuclear receptor steroidogenic factor 1 is essential for the formation of the ventromedial hypothalamic nucleus. Mol Endocrinol. 1995; 9:478–486. [PubMed: 7659091]

Ikeda Y, Takeda Y, Shikayama T, Mukai T, Hisano S, Morohashi KI. Comparative localization of Dax-1 and Ad4BP/SF-1 during development of the hypothalamic-pituitary-gonadal axis suggests their closely related and distinct functions. Dev Dyn. 2001; 220:363–376. [PubMed: 11307169]

Jacobowitz, DM.; Abbott, LC. Chemoarchitectonic atlas of the developing mouse brain. Boca Raton, FL: CRC Press; 1998.

Kim KW, Zhao L, Parker KL. Central nervous system-specific knockout of steroidogenic factor 1. Mol Cell Endocrinol. 2009; 300:132–136. [PubMed: 18951950]

Kim KW, Li S, Zhao H, Peng B, Tobet SA, Elmquist JK, Parker KL, Zhao L. CNS-specific ablation of steroidogenic factor 1 results in impaired female reproductive function. Mol Endocrinol. 2010; 24:1240–1250. [PubMed: 20339005]

Kim KW, Zhao L, Donato J Jr, Kohno D, Xu Y, Elias CF, Lee C, Parker KL, Elmquist JK. Steroidogenic factor 1 directs programs regulating diet-induced thermogenesis and leptin action in the ventral medial hypothalamic nucleus. Proc Natl Acad Sci U S A. 2011; 108:10673–10678. [PubMed: 21636788]

King BM. The rise, fall, and resurrection of the ventromedial hypothalamus in the regulation of feeding behavior and body weight. Physiol Behav. 2006; 87:221–244. [PubMed: 16412483]

Klockener T, Hess S, Belgardt BF, Paeger L, Verhagen LA, Husch A, Sohn JW, Hampel B, Dhillon H, Zigman JM, Lowell BB, Williams KW, Elmquist JK, Horvath TL, Kloppenburg P, Bruning JC. High-fat feeding promotes obesity via insulin receptor/PI3K-dependent inhibition of SF-1 VMH neurons. Nat Neurosci. 2011; 14:911–918. [PubMed: 21642975]

Kow LM, Pfaff DW. Mapping of neural and signal transduction pathways for lordosis in the search for estrogen actions on the central nervous system. Behav Brain Res. 1998; 92:169–180. [PubMed: 9638959]

Krieger MS, Conrad LC, Pfaff DW. An autoradiographic study of the efferent connections of the ventromedial nucleus of the hypothalamus. J Comp Neurol. 1979; 183:785–815. [PubMed: 762273]

Kurrasch DM, Cheung CC, Lee FY, Tran PV, Hata K, Ingraham HA. The neonatal ventromedial hypothalamus transcriptome reveals novel markers with spatially distinct patterning. J Neurosci. 2007; 27:13624–13634. [PubMed: 18077674]

Lopez M, Varela L, Vazquez MJ, Rodriguez-Cuenca S, Gonzalez CR, Velagapudi VR, Morgan DA, Schoenmakers E, Agassandian K, Lage R, Martinez de Morentin PB, Tovar S, Nogueiras R, Carling D, Lelliott C, Gallego R, Oresic M, Chatterjee K, Saha AK, Rahmouni K, Dieguez C,

Vidal-Puig A. Hypothalamic AMPK and fatty acid metabolism mediate thyroid regulation of energy balance. Nat Med. 2010; 16:1001–1008. [PubMed: 20802499]

McClellan KM, Parker KL, Tobet S. Development of the ventromedial nucleus of the hypothalamus. Front Neuroendocrinol. 2006; 27:193–209. [PubMed: 16603233]

Millhouse OE. The organization of the ventromedial hypothalamic nucleus. Brain Res. 1973; 55:71–87. [PubMed: 4713193]

Morrison CD, Munzberg H. Capricious cre: the devil is in the details. Endocrinology. 2012; 153:1005–1007. [PubMed: 22355175]

Musatov S, Chen W, Pfaff DW, Kaplitt MG, Ogawa S. RNAi-mediated silencing of estrogen receptor α in the ventromedial nucleus of hypothalamus abolishes female sexual behaviors. Proc Natl Acad Sci U S A. 2006; 103:10456–10460. [PubMed: 16803960]

Nagy A. Cre recombinase: the universal reagent for genome tailoring. Genesis. 2000; 26:99–109. [PubMed: 10686599]

Narita K, Murata T, Honda K, Nishihara M, Higuchi T, Takahashi M. Efferent pathways involved in the running activity originate in the ventromedial hypothalamus of the rat. Ann N Y Acad Sci. 1998; 860:556–559. [PubMed: 9928362]

Padilla SL, Carmody JS, Zeltser LM. Pomc-expressing progenitors give rise to antagonistic neuronal populations in hypothalamic feeding circuits. Nat Med. 2010; 16:403–405. [PubMed: 20348924]

Padilla SL, Reef D, Zeltser LM. Defining POMC neurons using transgenic reagents: impact of transient pomc expression in diverse immature neuronal populations. Endocrinology. 2012; 153:1219–1231. [PubMed: 22166984]

Paxinos, G. Atlas of the developing mouse brain at E17.5, P0 and P6. Amsterdam: Elsevier; 2007.

Ramadori G, Fujikawa T, Anderson J, Berglund ED, Frazao R, Michan S, Vianna CR, Sinclair DA, Elias CF, Coppari R. SIRT1 deacetylase in SF1 neurons protects against metabolic imbalance. Cell Metab. 2011; 14:301–312. [PubMed: 21907137]

Risold PY, Canteras NS, Swanson LW. Organization of projections from the anterior hypothalamic nucleus: a *Phaseolus vulgaris*-leucoagglutinin study in the rat. J Comp Neurol. 1994; 348:1–40. [PubMed: 7814679]

Saper CB, Swanson LW, Cowan WM. The efferent connections of the ventromedial nucleus of the hypothalamus of the rat. J Comp Neurol. 1976; 169:409–442. [PubMed: 61975]

Schambra, UB. Prenatal mouse brain atlas. New York: Springer; 2008.

Shimada M, Nakamura T. Time of neuron origin in mouse hypothalamic nuclei. Exp Neurol. 1973; 41:163–173. [PubMed: 4743483]

Shinoda K, Lei H, Yoshii H, Nomura M, Nagano M, Shiba H, Sasaki H, Osawa Y, Ninomiya Y, Niwa O, et al. Developmental defects of the ventromedial hypothalamic nucleus and pituitary gonadotroph in the Ftz-F1 disrupted mice. Dev Dyn. 1995; 204:22–29. [PubMed: 8563022]

Simerly RB, Chang C, Muramatsu M, Swanson LW. Distribution of androgen and estrogen receptor mRNA-containing cells in the rat brain: an in situ hybridization study. J Comp Neurol. 1990; 294:76–95. [PubMed: 2324335]

Sternson SM, Shepherd GM, Friedman JM. Topographic mapping of VMH→arcuate nucleus microcircuits and their reorganization by fasting. Nat Neurosci. 2005; 8:1356–1363. [PubMed: 16172601]

Tobet SA, Henderson RG, Whiting PJ, Sieghart W. Special relationship of gamma-aminobutyric acid to the ventromedial nucleus of the hypothalamus during embryonic development. J Comp Neurol. 1999; 405:88–98. [PubMed: 10022198]

Tong Q, Ye C, McCrimmon RJ, Dhillon H, Choi B, Kramer MD, Yu J, Yang Z, Christiansen LM, Lee CE, Choi CS, Zigman JM, Shulman GI, Sherwin RS, Elmquist JK, Lowell BB. Synaptic glutamate release by ventromedial hypothalamic neurons is part of the neurocircuitry that prevents hypoglycemia. Cell Metab. 2007; 5:383–393. [PubMed: 17488640]

Tran PV, Lee MB, Marin O, Xu B, Jones KR, Reichardt LF, Rubenstein JR, Ingraham HA. Requirement of the orphan nuclear receptor SF-1 in terminal differentiation of ventromedial hypothalamic neurons. Mol Cell Neurosci. 2003; 22:441–453. [PubMed: 12727442]

Tran PV, Akana SF, Malkovska I, Dallman MF, Parada LF, Ingraham HA. Diminished hypothalamic bdnf expression and impaired VMH function are associated with reduced SF-1 gene dosage. J Comp Neurol. 2006; 498:637–648. [PubMed: 16917842]

Xu Y, Hill JW, Fukuda M, Gautron L, Sohn JW, Kim KW, Lee CE, Choi MJ, Lauzon DA, Dhillon H, Lowell BB, Zigman JM, Zhao JJ, Elmquist JK. PI3K signaling in the ventromedial hypothalamic nucleus is required for normal energy homeostasis. Cell Metab. 2010; 12:88–95. [PubMed: 20620998]

Xu Y, Nedungadi TP, Zhu L, Sobhani N, Irani BG, Davis KE, Zhang X, Zou F, Gent LM, Hahner LD, Khan SA, Elias CF, Elmquist JK, Clegg DJ. Distinct hypothalamic neurons mediate estrogenic effects on energy homeostasis and reproduction. Cell Metab. 2011; 14:453–465. [PubMed: 21982706]

Yi CX, Scherer T, Tschop MH. Cajal revisited: does the VMH make us fat? Nat Neurosci. 2011; 14:806–808. [PubMed: 21709675]

Yokawa T, Mitsushima D, Itoh C, Konishi H, Shiota K, Takahashi M. The ventromedial nucleus of the hypothalamus outputs long-lasting running in rats. Physiol Behav. 1989; 46:713–717. [PubMed: 2602498]

Zhang R, Dhillon H, Yin H, Yoshimura A, Lowell BB, Maratos-Flier E, Flier JS. Selective inactivation of Socs3 in SF1 neurons improves glucose homeostasis without affecting body weight. Endocrinology. 2008; 149:5654–5661. [PubMed: 18669597]

Zhao L, Kim KW, Ikeda Y, Anderson KK, Beck L, Chase S, Tobet SA, Parker KL. Central nervous system-specific knockout of steroidogenic factor 1 results in increased anxiety-like behavior. Mol Endocrinol. 2008; 22:1403–1415. [PubMed: 18372344]

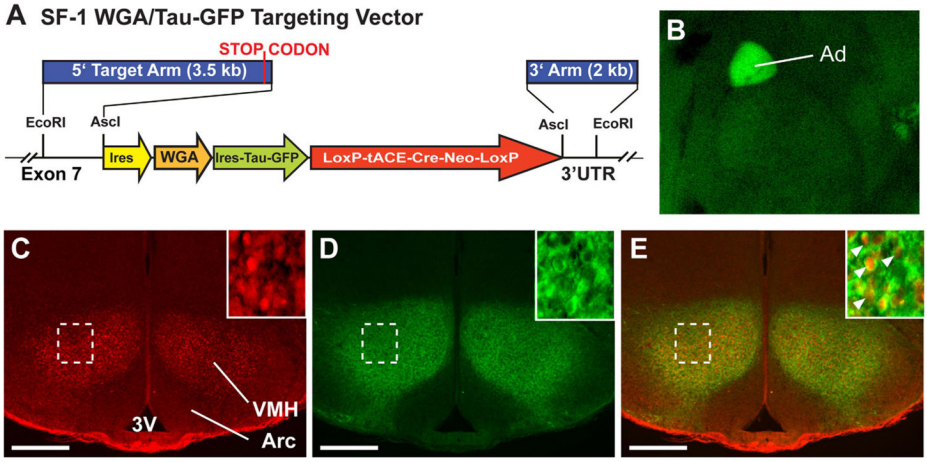

Figure 1.

A: Schematic of the *Sf-1*^{TauGFP} knock-in targeting vector positioned in the mouse *nr5a1* (*Sf-1*) locus. **B**: Fluorescence image of the adrenal gland in the *Sf-1*^{TauGFP} knock-in mouse. **C–E**: Photomicrographs of nuclear immunostaining of SF-1 (C), cytoplasmic immunostaining of GFP (D), and their colocalization in the VMH at P0 (E). **Insets** show higher magnifications of the boxed areas and with SF-1 and GFP colocalized in neurons (arrowheads). Scale bars = 0.25 mm.

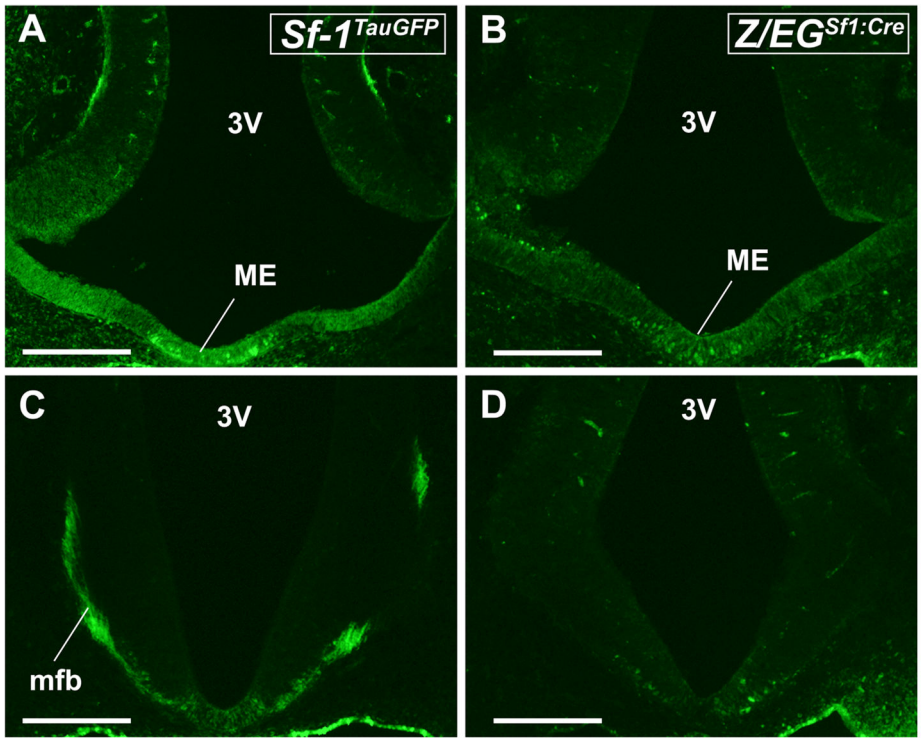

Figure 2.

Coronal brain sections from *Sf-1*^{TauGFP} mouse (A,C) and *Z/EG*$^{Sf1:Cre}$ mouse (B,D) at E10.5. **A,B**: GFP-labeled neurons are present in the median eminence (ME) of the *Sf-1*^{TauGFP} mouse. **C,D**: GFP-labeled fibers in the medial forebrain bundle (mfb) of the *Sf-1*^{TauGFP} mouse but not the *Z/EG*$^{Sf1:Cre}$ mouse. 3V, third ventricle. Scale bars = 0.5 mm.

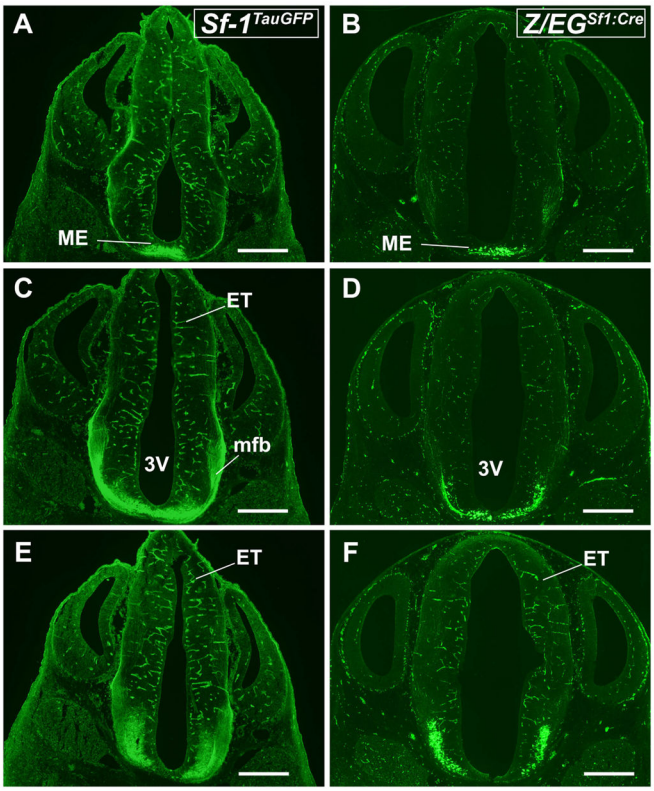

Figure 3.

Anterior to posterior coronal brain sections from *Sf-1*^{TauGFP} mouse (A,C,E) and *Z/EG*$^{Sf1:Cre}$ reporter mouse (B,D,F) at E12.5. **A,B**: GFP-stained neurons in the median eminence (ME). **C,D**: GFP-labeled neurons in the ME with fibers traveling in the medial forebrain bundle (mfb) in the *Sf-1*^{TauGFP} mouse but not in the *Z/EG*$^{Sf1:Cre}$ mouse. **E,F**: GFP-stained neurons in the presumptive VMH and fibers in *Sf-1*^{TauGFP} mice. Scale bars = 0.75 mm.

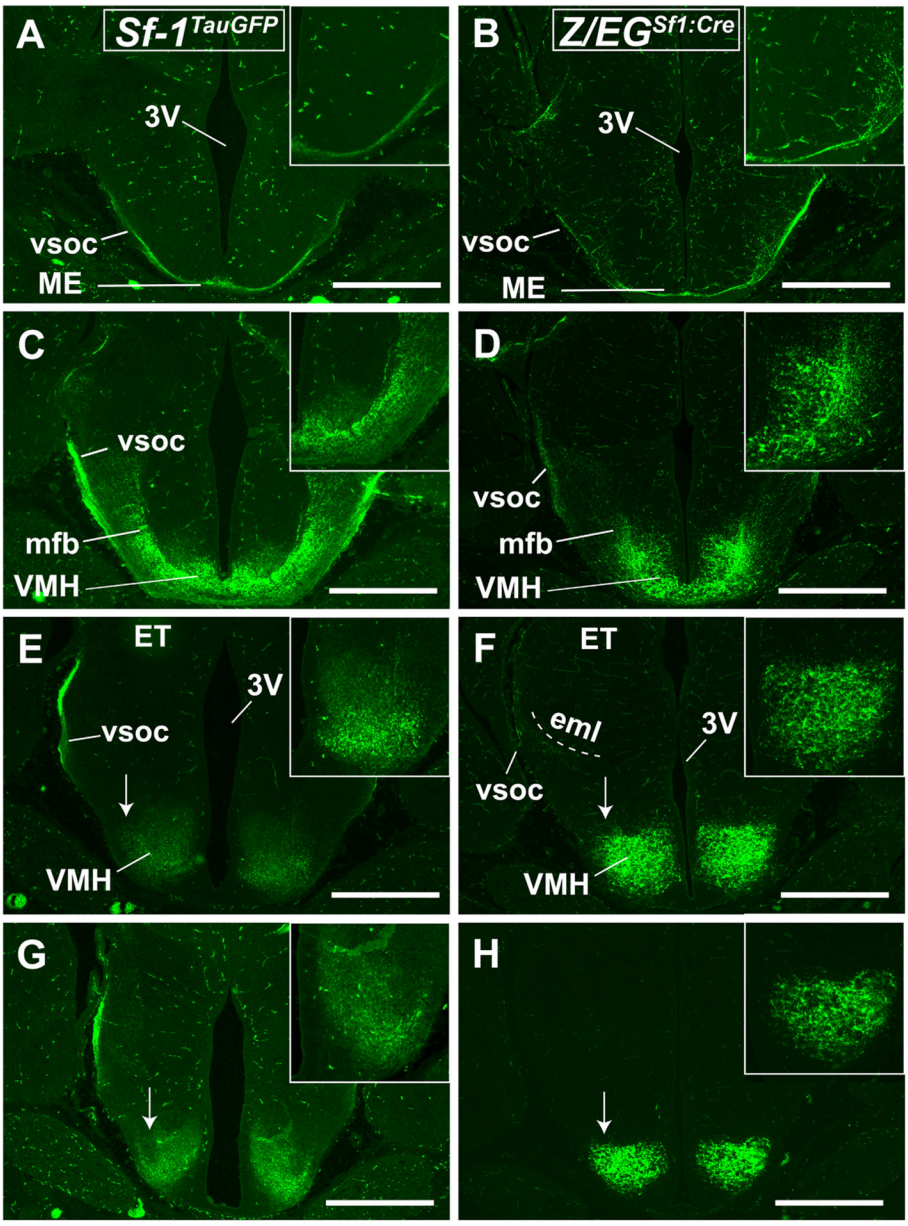

Figure 4.

Anterior to posterior coronal brain sections from *Sf-1*^{TauGFP} mouse (A,C,E,G) and *Z/EG*$^{Sf1:Cre}$ reporter mouse (B,D,F,H) at E 14.5. **A,B**: Fibers in the ME and extending into the ventral supraoptic commissure (vsoc). **C,D**: GFP-stained neurons in the VMH and fibers tracts extending dorsally along the vsoc. E,F: Fibers traveling in the mfb angle toward and join the vsoc at the level of the external medullary lamina (eml). **E–H**: The ventrolateral aspect of the VMH in *Sf-1*^{TauGFP} (E,G) and in *Z/EG*$^{Sf1:Cre}$ mice (F,H) is indicated by arrows. **Insets** show expanded view of the VMH and its efferent fibers. Scale bars = 0.5 mm.

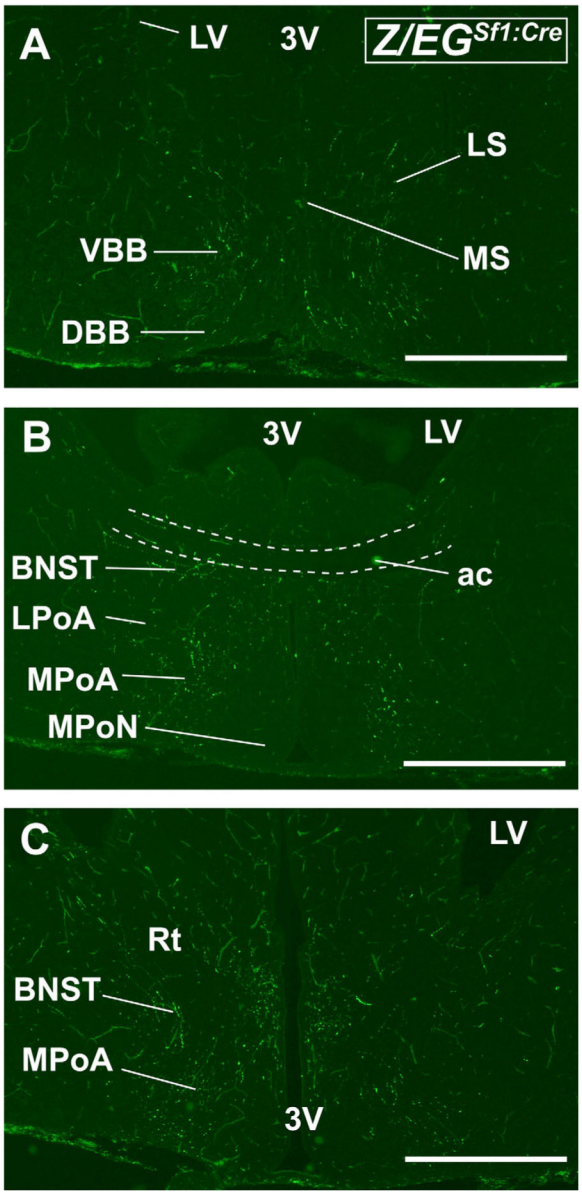

Figure 5.

Anterior coronal brain sections from the *Z/EG*$^{Sf1:Cre}$ mouse at E 17.5. **A**: Fibers are detected in the vertical band of Broca (VBB), the diagonal band of Broca (DBB), and the lateral septal nucleus (LS). Scant fibers are found in the medial septal nucleus (MS). **B**: Fibers can be seen in the bed nucleus of stria terminalis (BNST) and medial preoptic area (MPoA), sparing the lateral preoptic area (LPoA) and the medial preoptic nucleus (MPoN). **C**: Fibers are seen in the BNST, by the reticular nucleus of the thalamus (Rt), and in MPoA as well as in the periventricular zone of the third ventricle (3V). Scale bars = 0.5 mm.

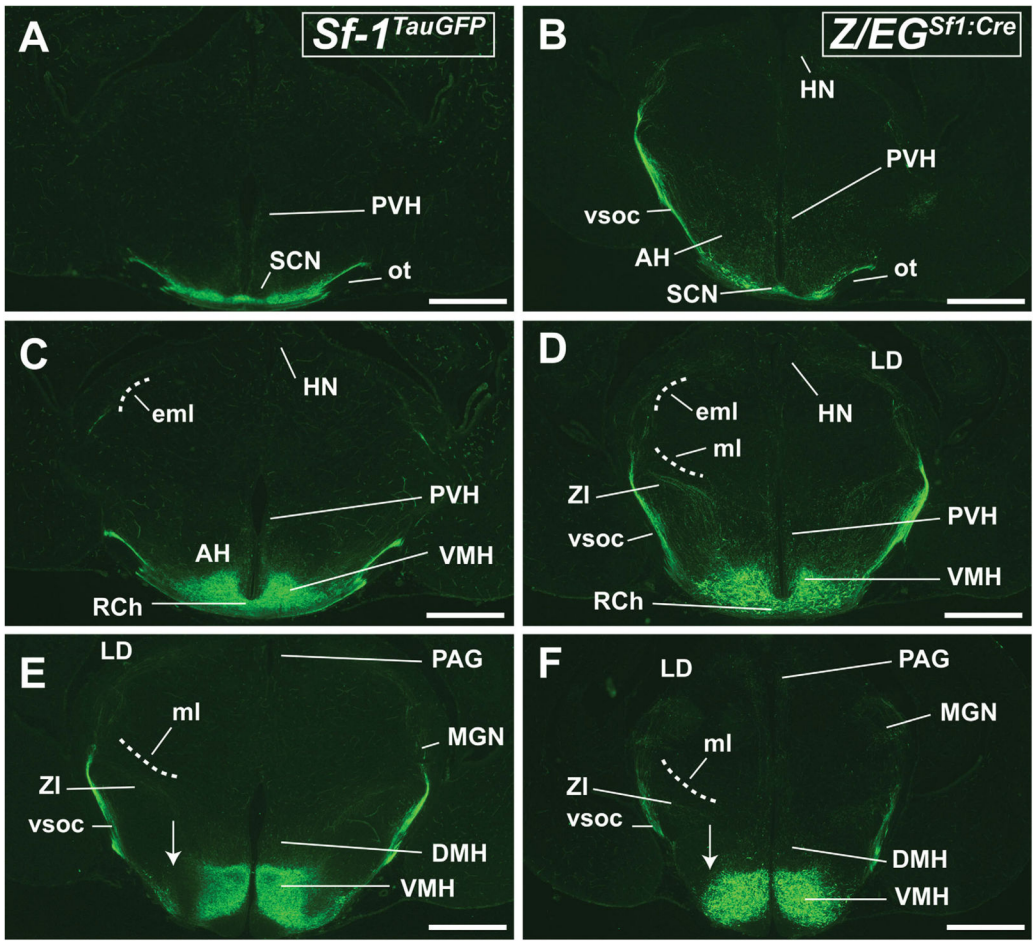

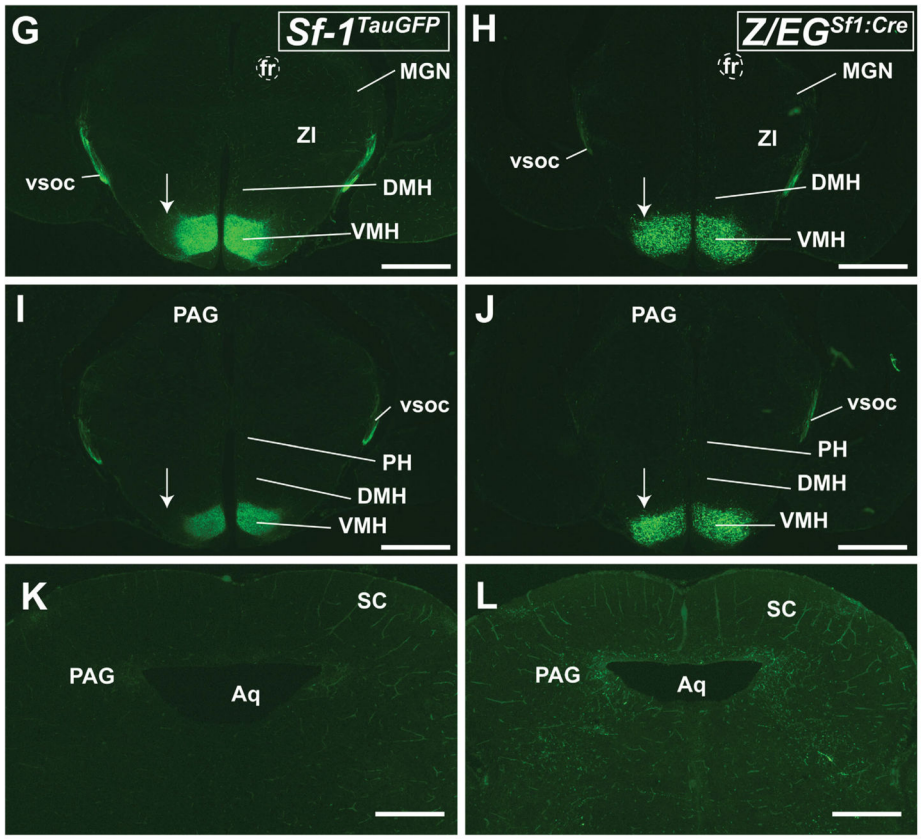

Figure 6.

Anterior to posterior coronal brain sections from the *Sf-1*^{TauGFP} mouse (A,C,E,G,I,K) and the *Z/EG*$^{Sf1:Cre}$ reporter mouse (B,D,F,H,J,L) at E 17.5. **A,B**: Fibers are seen surrounding, but sparing, the suprachiasmatic nucleus (SCN) in both mouse models. Hypothalamic paraventricular nucleus (PVH) and the anterior hypothalamus (AH) also receive fiber projections. The vsoc is the major fiber tract and travels laterally and dorsally. **C,D**: Fine fiber tracts are seen projecting toward the HN and the PVH. **E,F**: Fibers projecting from the dorsolateral region of the VMH join the vsoc at the lateral aspect of the medial lemniscus (ml). Midline fibers travel through the dorsomedial hypothalamic nucleus (DMH) to terminate in the periaqueductal gray (PAG), whereas lateral fibers fanning out from the vsoc travel through the medial geniculate nucleus (MGN). Arrows point to the ventrolateral region of the VMH (VMH_{vl}), where GFP^+ neurons are present in the *Z/EG*$^{Sf1:Cre}$ reporter mouse but not the *Sf-1*^{TauGFP} mouse. **G–J**: GFP^+ neurons in the VMH_{vl} are absent in the *Sf-1*^{TauGFP} mouse (G,I) but present in the *Z/EG*$^{Sf1:Cre}$ mouse (H,J). Fibers travel through the posterior hypothalamus (PH) and the DMH medially and the MGN laterally. **K,L**: Fibers can be seen in the PAG and deeper layer of the superior colliculus (SC). For abbreviations see list. Scale bars = 0.5 mm.

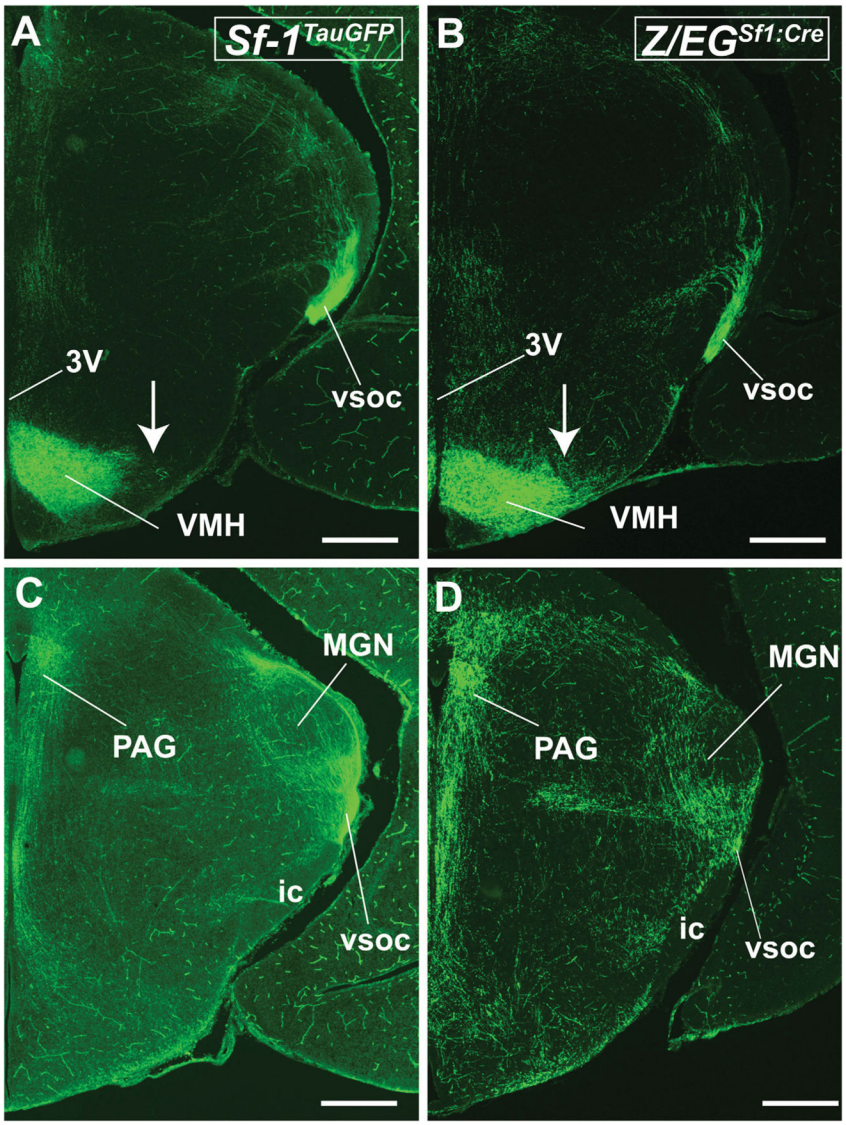

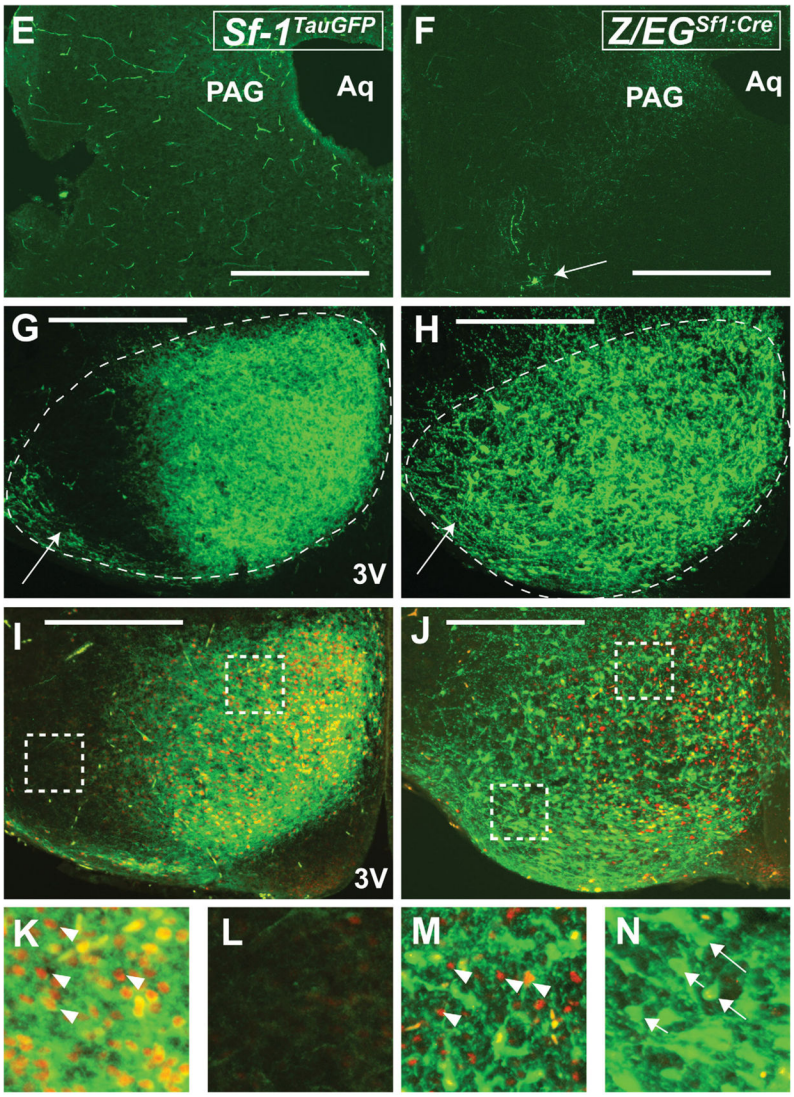

Figure 7.

Comparisons between the *Sf-1*^{TauGFP} mouse (A,C,E,G,I,K,L) and the *Z/EG*$^{Sf1:Cre}$ mouse (B,D,F,H,J,M,N) at P0. **A,B**: Comparable projection patterns are seen in the vsoc and fibers traveling in the periventricular system. Cells are noticeably absent in the VMH_{vl} of the *Sf-1*^{TauGFP} mouse compared with the corresponding region in the *Z/EG*$^{Sf1:Cre}$ mouse (arrow). **C,D**: Similar fiber projections are seen in the vsoc along the internal capsule (ic), across the medial geniculate nucleus (MGN), and into the PAG. **E,F**: Fiber projections are seen in the PAG. A solitary GFP^+ cell can be seen in the tegmental area of the midbrain of the *Z/EG*$^{Sf1:Cre}$ (arrow in F). **G,H**: Absence of GFP^+ cells in the VMH_{vl} of the *Sf-1*^{TauGFP} mouse (G). Arrows indicate the presence of GFP^+ cells in the presumptive tuberal region of both mouse models. **I,J**: Colabeling of cytoplasmic GFP^+ staining (green) and nuclear $SF\text{-}1^+$ staining (red) in the VMH. Absence of $SF\text{-}1^+$ staining is noted in the VMH_{vl} of both mouse lines. Boxed areas are shown as expanded views in K–N. **K,L**: Expanded views of the VMH in *Sf-1*^{TauGFP} mice from Figure 7I showing colabeling (arrowheads) in the compact region (K) and the absence of any labeling in the VMH_{vl} (L). **M,N**: Expanded views of the VMH in

the *Z/EG*$^{Sf1:Cre}$ mouse from Figure 7J showing colabeling (arrowheads) in the compact region (M) with only GFP^{+} labeling (arrows) in the VMH_{vl} (N). For abbreviations see list. Scale bars = 0.5 mm.

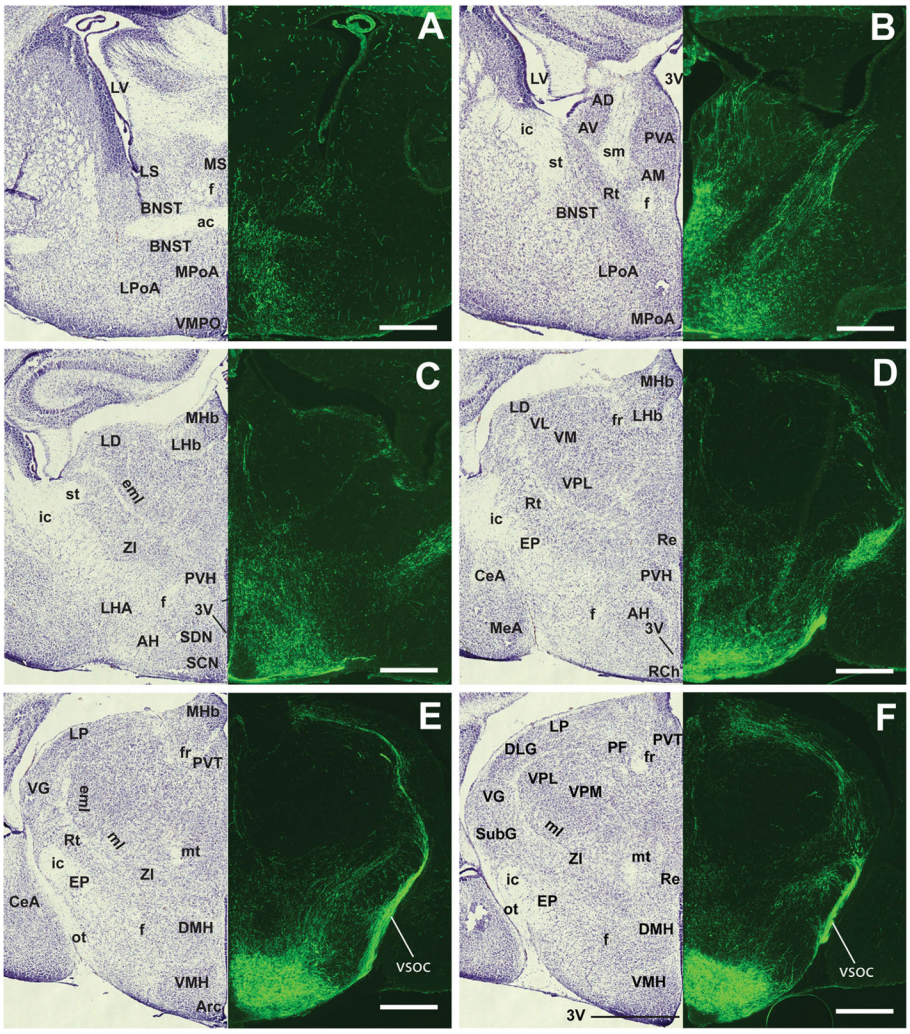

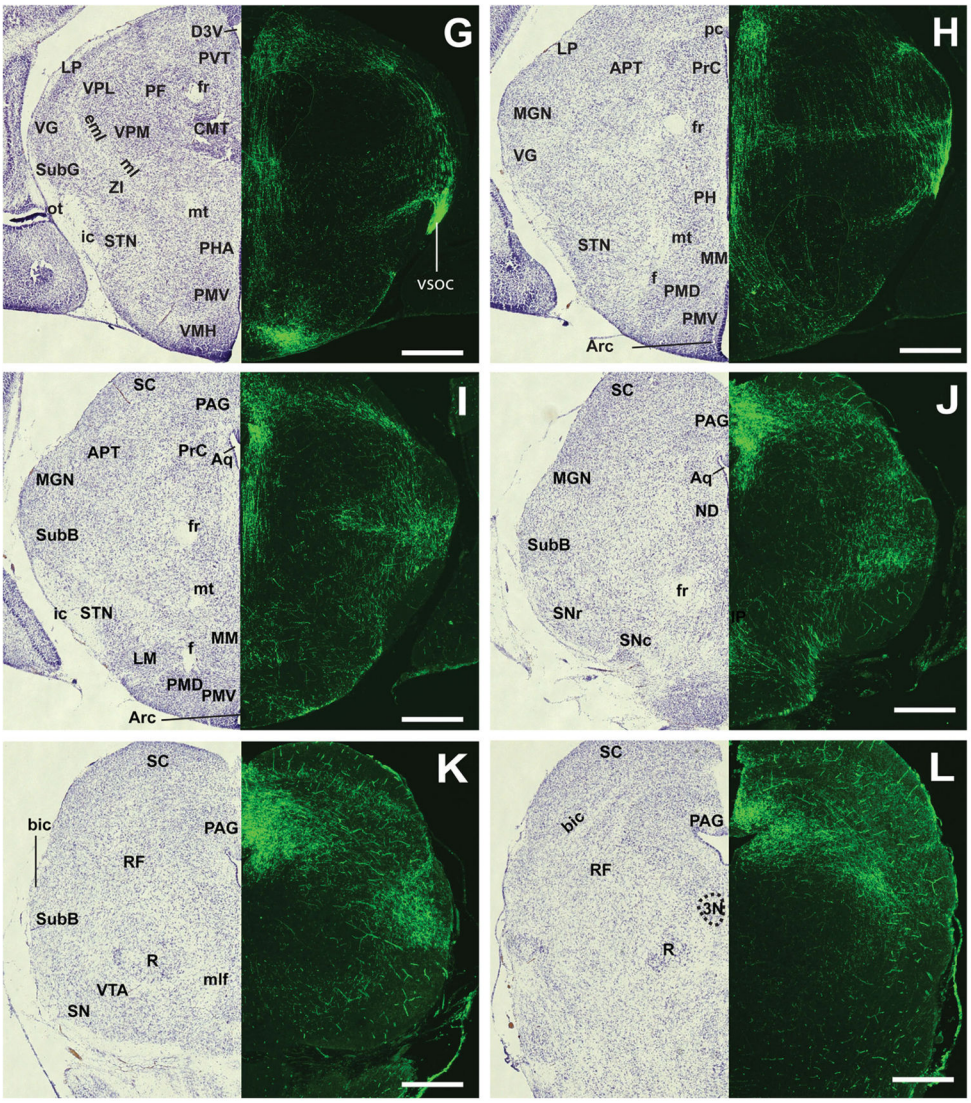

Figure 8.

Anterior to posterior coronal brain sections from the *Z/EG*$^{Sf1:Cre}$ reporter mouse at P0. **A–R**: Projection patterns of GFP-labeled fibers (right) and the corresponding contralateral Nissl-stained sections (left). **S–U**: High-power photomicrographs showing the corresponding amygdaloid nuclei in the field of GFP-labeled fibers. For abbreviations see list. Scale bars = 0.675 mm in A–R; 0.25 mm in S–U.

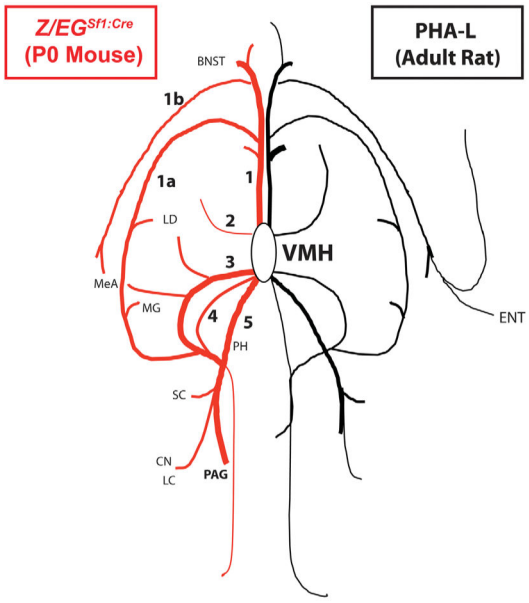

Figure 9.

Simplified graphic representation of the fiber projection patterns in the *Z/EG*$^{Sf1:Cre}$ reporter mouse at P0 and the PHA-L-injected rat at the adult stage, modified from Canteras et al. (1994). For abbreviations see list. ENT, entorhinal area.

TABLE 1

Primary Antibodies Used

Antigen	Immunogen	Raised in	Manufacturer data	IHC dilution
GFP	Purified recombinant GFP	Chicken polyclonal	Aves Labs (GFP-1020)	1:2,500 (TSA), 1:200 (non-TSA)
SF-1	Purified recombinant SF-1 hinge LBD	Rabbit polyclonal	Bio.Synthesis (custom made)	1:100

TABLE 2

VMH Developmental Profiles

Tract/region	Reporter line	E10.5	E12.5	E14.5	E17.5	P0
MFB	*Sf-1*^{TauGFP}	+	++	+++	++	++
	Z/EG$^{Sf1::Cre}$	–	+	+	++	++
vSOC	*Sf-1*^{TauGFP}	+/–	+	++	+++	+++
	Z/EG$^{Sf1::Cre}$	–	+/–	+	++	+++
GFP^{+} neurons	*Sf-1*^{TauGFP}	+	++	++	+++	+++
	Z/EG$^{Sf1::Cre}$	+/–	+	++	+++	+++
GFP^{+} in the VMH$_{vl}$	*Sf-1*^{TauGFP}	ND	ND	+/–	–	–
	Z/EG$^{Sf1::Cre}$	ND	ND	+	+	+